Gravimetric Definition of the Magmatic Chambers of the Popocatépetl-Iztaccíhuatl Volcanic Complex, Mexico

Román Alvarez[1, *], Miguel Camacho-Ascanio[2]

[1]Applied Mathematics and Systems Research Institute, National Autonomous University of Mexico, Mexico City 04510, Mexico

[2]Department of Earth Sciences, National Autonomous University of Mexico, Mexico City 04510, Mexico

Abstract: Volcanic activity is a potential hazard when activity occurs near populated regions. Iztaccíhuatl (IZ) and Popocatépetl (PO) volcanoes are in the Trans Mexican Volcanic Belt, in the Sierra Nevada range, near populated areas reaching nearly 28 million people. Understanding their internal structures may help prevent catastrophic consequences. To explore the relationship between their plumbing systems we perform 3D inversions of its high-resolution, satellite-derived Bouguer anomaly, which unveils heretofore unknown relationships between them. Previous gravity analyses suggest the existence of an extensional process whose axis is along the Sierra Nevada, including the area of Mexico City to the NW, and extending beyond Malinche volcano to the SE. Different resolutions of the volume inversions help visualize the internal structures of PO and IZ. The inversion with the highest resolution shows the IZ volcano displaying two magma chambers along the N-S direction. The main magma chamber is fed vertically from deeper sources, whilst the adjacent one is apparently fed horizontally from the main one. PO's magma chamber is not fed vertically, but at ~21° from the vertical, by the main magmatic chamber of IZ; the center of PO's magmatic chamber is located at +1.8 km asl. The present chimney of PO is observed to deflect from the vertical, which we associate with the collapse of an ancestral volcano of PO, recognized as El Ventorrillo. The present chimney of PO drastically diminishes its cross-section 3 km asl, risking occlusion, which may lead to an explosive event. These findings agree with the seismic and geobarometric results obtained elsewhere.

Keywords: Sierra Nevada; Popocatépetl; Iztaccíhuatl; Malinche Volcano; Satellite-derived Gravity; 3D Gravity Inversions; Magma Chambers; Plumbing Systems

DOI: 10.57237/j.earth.2025.01.001

1 Introduction

Popocatépetl (PO) and Iztaccíhuatl (IZ) volcanoes are in the Trans Mexican Volcanic Belt and belong to a roughly N-S alignment of volcanic structures named the Sierra Nevada in central Mexico [1]. These structures have been studied individually [2-4], or as part of the Sierra Nevada range [1, 5].

The relevance of PO volcano rests not only in its present, continuous activity, but also in its proximity to densely populated areas that can be affected by its eruptions, which include pyroclastic surges, fumarolic activity, lahars, and lava flows [4, 7, 8, 37]; volcanic activity resumed in 1994 after a long period of quiescence [2, 9, 36]. Emission of gas and steam fumaroles shifting with ash-rich plumes rising to 4–8 km above the summit crater

*Corresponding author: Román Alvarez, roman.alvarez@iimas.unam.mx

Received: 13 January 2025; Accepted: 4 March 2025; Published Online: 17 April 2025

were the initial manifestations [10], followed by an almost continuous activity to date [4, 35]. The architecture of the PO's plumbing system [3] has remained stable throughout the last ∼14.1 ka, and magma environments have sustained above-solidus magma storage temperatures in the lower to mid-crust at 1080–1220 ℃.

A study of the Sierra Nevada range [5] includes, in addition to PO and IZ, volcanoes Tláloc and Telapón that belong to the same N-S range. The K-Ar dates of various volcanic ejecta indicate the activity of the four volcanoes has been contemporaneous during most of the Middle to Late Pleistocene. Activity has migrated southwards since it started 1.8 Ma at Tláloc [5], the northernmost volcano of the range, extending southwards with IZ at 1 Ma [11]. The latter publication suggested that regional crustal tectonics played a secondary role in the N-S alignment of the volcanoes, whilst Cocos plate rollback is mainly responsible for it. After subduction in the Middle America Trench, the Cocos plate is horizontal (i.e., not subducting) in a large extent before reaching the Sierra Nevada region, where it experiences a rollback. An extensional process was described [12] with apparent axis located at Sierra Nevada under the portion of the volcanic belt below Sierra Nevada.

Based on the study of clinopyroxene geobarometers, analysis of temperature vs pressure characteristics of PO were made [13], using a proposed plumbing system [14]; the association of the composition of these minerals to pressure/depth diagrams and the diagrammatic plumbing system, identified three different reservoirs in Popocatépetl volcano: the deepest close to the base of the crust (~-30 km), the intermediate at ~-18 km elevation, and the uppermost at ~-10-0 km elevation. They show a schematic model of the plumbing system; their model shows the vertical uprising of the magma through the crust. In the present work, we model the uppermost magmatic chamber via gravimetric determinations, generating models at various spatial resolutions, and superposing temperature vs pressure determinations [13].

Here we model Popocatépetl and Iztaccíhuatl volcanoes (Figure 1) using a high-resolution gravity data set, to perform an inversion of the complete Bouguer anomaly of this volcanic complex. The term *ultra-high-resolution gravity* was coined by Hirt et al. [15]. The modeling procedure essentially consists of a 3D inversion of the volcanoes' high-resolution gravity field (Bouguer anomaly) obtained from the satellite-derived data in mGal [15]; this procedure yields the density distribution in g/cm^3 in the volcano's interior, allowing to uncover the characteristics of its plumbing system. We use three model resolutions to highlight different aspects of the volcanic structures: 1000, 500, and 250 m. The process to obtain the Bouguer anomaly was described [16], and examples of similar 3D inversions in volcanic structures are available in the literature [17-20]. Modeling with satellite-derived gravity data often raises questions about the validity of the data. We include here a brief description of the procedure to help unfamiliar readers with this subject grasp the essentials of the concepts involved. The calculation of gravity in the GGMplus model is carried out by combining satellite, terrestrial, and topographic gravity data, using massive parallel computing techniques. First, the most recent gravity data measured by the GOCE and GRACE satellites are incorporated, providing information at spatial scales of ~10000 to ~100 km. Then, data from the EGM2008 model, which covers scales from ~100 to ~10 km in the geoid, are added [15, 21]. From 10 km to 250 meters, we have the EGM2008 gravimetric model, which integrates different types of data (satellite, terrestrial, airborne, and marine) and achieves resolutions close to 1 km. Meanwhile, the range from 1 km to 250 meters is covered by the topographic gravity model. An example can be found of the use of satellite data versus terrestrial data [22].

Finally, terrestrial, airborne, and marine data from the EGM2008 model are integrated, combining them with gravimetry calculated from high-resolution topographic models, using a technique called topographic gravity, which is derived from high-resolution terrain models and complements scales from ~10 km to ~250 m [15]. This integrated approach allows for the generation of an ultra-high-resolution gravity model with a spatial precision of 7.2 arc-seconds (~200 m in the north-south direction), and an accuracy ranging from 2 to 5 mGal [15], although this depends on the quality of the topographic model in the area and the gravimetric data collected for the model. For example, in Africa, the average difference is usually 8 mGal compared to ground measurements.

Topographic gravity is based on a calculation with an assumed mass density of 2670 kg/m^3 and provides spatial scales from ~10 km to ~250 m. The conversion from topography to topographic gravity is performed using the residual terrain modeling technique [23], with high frequency filtered topography through the subtraction of a spherical harmonic reference surface (of degree and order 2160) before direct modeling. In this procedure, large water masses are converted into equivalent rock layers using a combination of residual terrain modeling with the concept of equivalent rock topography [15]. The short-scale value is a combination of values, which uses the satellite anomaly from the GOCE and GRACE missions as a base, and then combines the EGM2008 model (satellite, airborne, terrestrial, and marine), along with the addition of the gravity model generated by topographic gravimetry. These procedures generate short-scale topographic gravity that is suitable for extending spherical harmonic gravity models of degree 2190 beyond their associated resolution [24, 34].

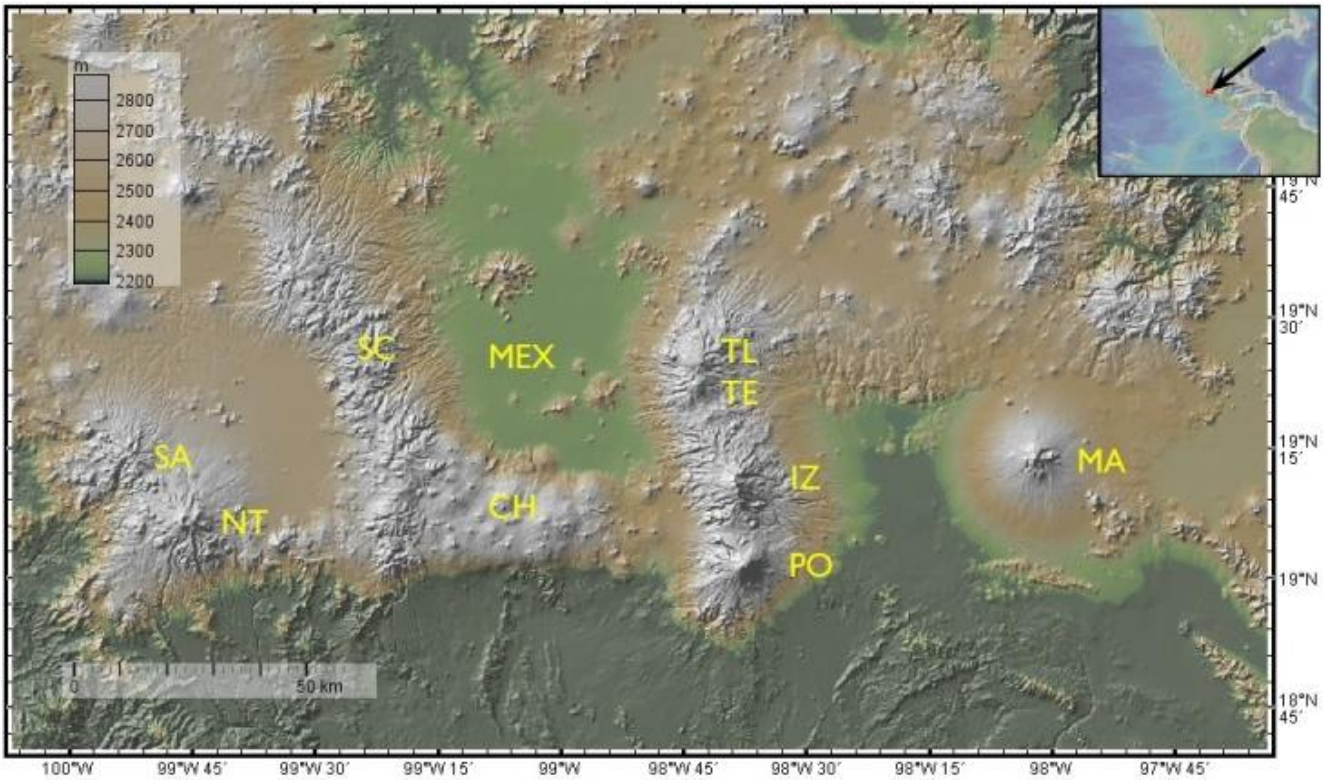

Figure 1 Digital Elevation Model (DEM) of the study area. The main volcanic structures are identified, and the location of Mexico City is indicated. MEX, Mexico City; PO, Popocatépetl; IZ, Iztaccíhuatl; TL, Tláloc, TE, Telapón, MA, Malinche; CH, Chichinautzin; SC, Sierra de Las Cruces; NT, Nevado de Toluca; SA, San Antonio. The red rectangle corresponds to the area of the map in Figure 2. Map from GeomapApp [25]

Using satellite-derived data in the case of volcanoes offers the double advantage of covering the surveyed area with a uniform mesh of gravity stations, and the data is freely available. On the contrary, terrestrial surveys are expensive and time consuming, and the risk is high of acquiring data in an active volcano; the stations in the volcanic slopes must follow trails that require subsequent interpolations to get a uniform mesh, which may introduce artifacts.

The objective of this study is to obtain gravity-derived models of the interior of two of the most important volcanoes in the Trans Mexican Volcanic Belt. Their importance derives not only from their size and ongoing activity, but also on their location near the largest population centers in Mexico.

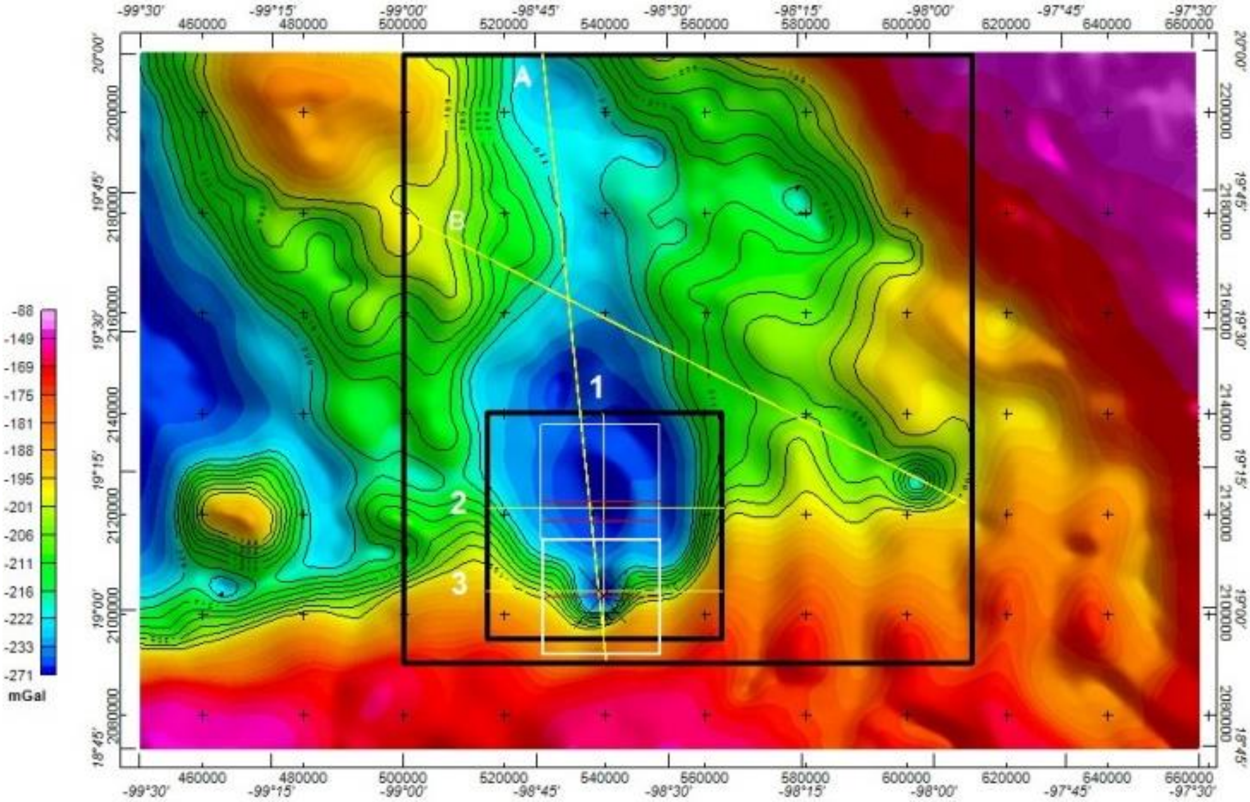

Figure 2 Complete Bouguer anomaly of the study area derived from the GGM+ gravity model; the map is enclosed in the DEM shown in Figure 1. UTM coordinates correspond to Zone 12N. Contour interval 6 mGal. The small, black rectangle comprises the Popocatépetl-Iztaccíhuatl region. Thin, yellow lines indicate the location of cross-sections 1, 2, and 3 within the small rectangle at a model resolution of 1000 m. The large, black rectangle marks the largest 3D inversion region, with a resolution of 2500 m reaching depths of ~17 km; cross-sections A and B are extracted from it. PO and IZ are located at the centers of the two white rectangles, which also locate the inverted regions for IZ and PO at 250-m resolution, and three E-W, red lines indicate the locations of the cross-sections obtained at that resolution. The corresponding N-S cross-sections follow the same path, as indicated by the yellow line associated with the small, black rectangle

2 Bouguer Anomaly Map

A general description of the characteristics of the Bouguer anomaly (BA) map in Figure 2 is in order. To the S and E, the region is surrounded by gravity highs. There are two regions showing gravity lows: in the central portion, the Popocatépetl-Iztaccíhuatl (PO-IZ) region, trending N-S, is one of them, and on the W portion another low is observed, corresponding to the Toluca Valley region. These gravity lows are separated by a gravity high that decreases in magnitude from N to S. A saddle point is in the vicinity of location 99° 00'W, 19° 15'N; from this point, values increase in the N-S direction and decrease in the E-W direction. A detailed gravity analysis of the Mexico Basin is available [12]. A series of gravity maxima, which alternate with parallel, gravity-lows is observed, with its axis along the Sierra Nevada; this arrangement of alternating high- and low-gravity sections suggests that the region is being or has been extended in the E-W direction, a process favoring the intrusion of magmatic materials, as observed in the PO-IZ region as well as associated with MA volcano. A more detailed analysis of the distribution of successive gravity highs and lows in this region will be performed further ahead.

Black squares in Figure 2 delimit the area in which 3D gravity inversions are performed. Lines labeled 1, 2, and 3 correspond to cross-sections obtained from the 3D inversion of the region indicated by the smaller, black square. These lines intersect the regions of lowest gravity values, which correspond to the Popocatépetl and Iztaccíhuatl summit locations. In these volcanoes there is an anti-correlation between topography and BA.

3 The Inversion Process

The inversion process transforms the Bouguer anomaly (mGal) into a density volume (g/cm^3). 3D gravity inversions rests on a method [26] based on appropriate theoretical considerations [27]. The code is implemented in the Oasis Montaj program of Geosoft. The program uses a Cartesian Cut Cell algorithm (CCC) to represent geologic volumes and an Iterative Reweighting Inversion algorithm (IRI) [28] to reproduce the observed results within established error limits, e.g. 0.5 mGal, or usually 5% of the standard deviation of the input data. Using an error limit of 0.2 mGal we obtained a correlation coefficient of +0.983 between the observed gravity data and the one produced by the inversion process. The depth of the inverted volume is proportional to the size of the volume selected for the calculation. Typically, choosing 500-m cubes will reach depths of 5-6 km; greater depths can be obtained at the expense of the resolution. To optimize computation, a subset of the high-resolution data set is used, selected according to the model resolution.

4 Results

4.1 Result of the 3D Inversion

A vertical cross-section of the inverted volume, under the summit of the volcanoes, is shown in Figure 3; it is directly located under the summits of IZ and PO volcanoes, displaying the low-density regions under the volcanic structures, identified as their plumbing systems and magma chambers. We distinguish between structural density lows and density lows of the volcanic system contextually and geometrically. Density lows may occur by the accumulation of sediments or, in the case of active volcanoes, by the accumulation of low-density magmatic products. The geologic context in which the accumulation occurs determines the type one should consider. The volume can be dissected in vertical, horizontal, or arbitrarily oriented planes to help visualize the distribution of densities (rock materials) of interest. We focus the analysis mostly on low-density materials since in the case of active volcanoes they are usually associated with storage and conduits of magmatic constituents. As shown in Figure 3, in the case of PO and IZ, these volcanoes are underlain by extensive deep formations of low-density materials, not only in the vertical plane shown but also on perpendicular planes that will be analyzed below at various model resolutions.

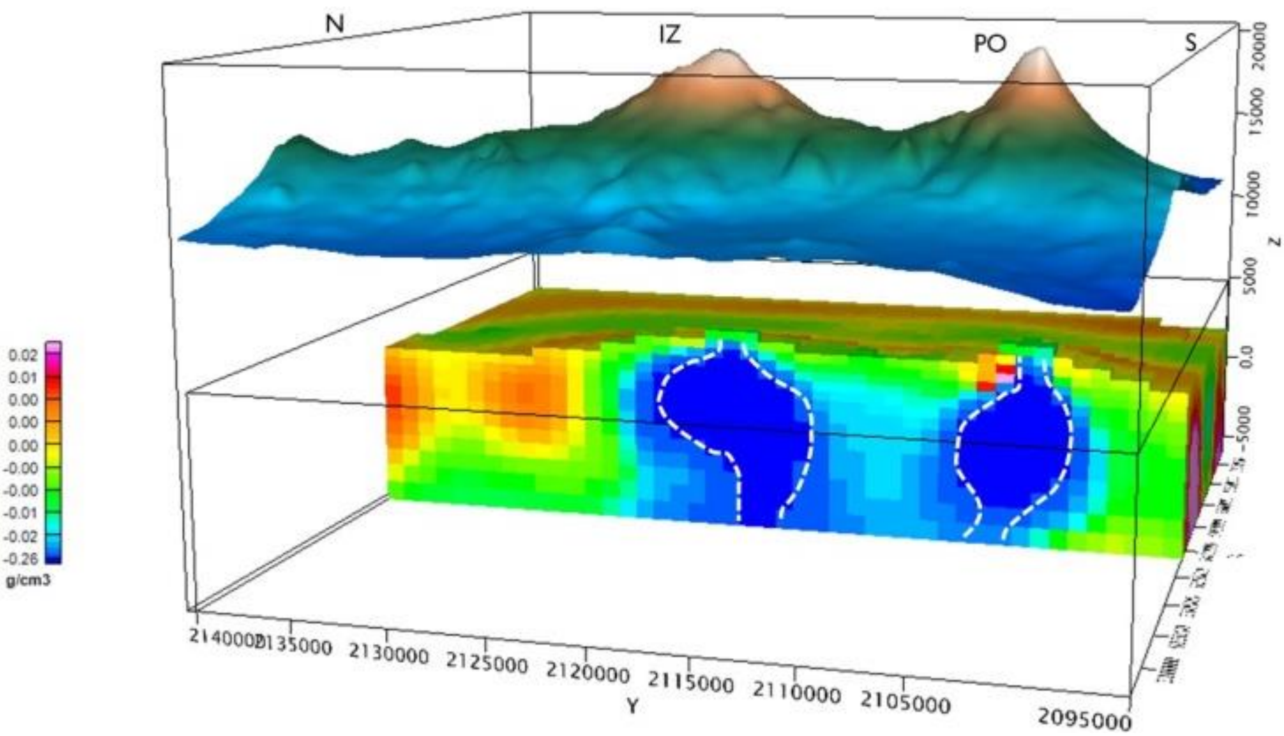

Figure 3 Density distribution (g/cm^3) obtained from the 3D inversion, with highlighted low-density regions (dashed lines) under IZ y PO volcanoes, identified as their corresponding plumbing systems and magma chambers. The inverted volume is clipped in a vertical Y-Z plane directly under the volcanoes' summits; the topographic profile of the inverted volume is averaged to the model resolution and can be discerned along the vertical plane shown. Notice the high-density region on the N flank of PO, which further ahead we associate with an ancestral volcanic edifice called El Ventorrillo. The DEM of the two volcanoes is displaced upward to allow a full view of the top of the inverted volume. Dashed, white lines indicate the regions of lowest density in the inverted volume. The view is from the west

4.2 Cross-section Analyses

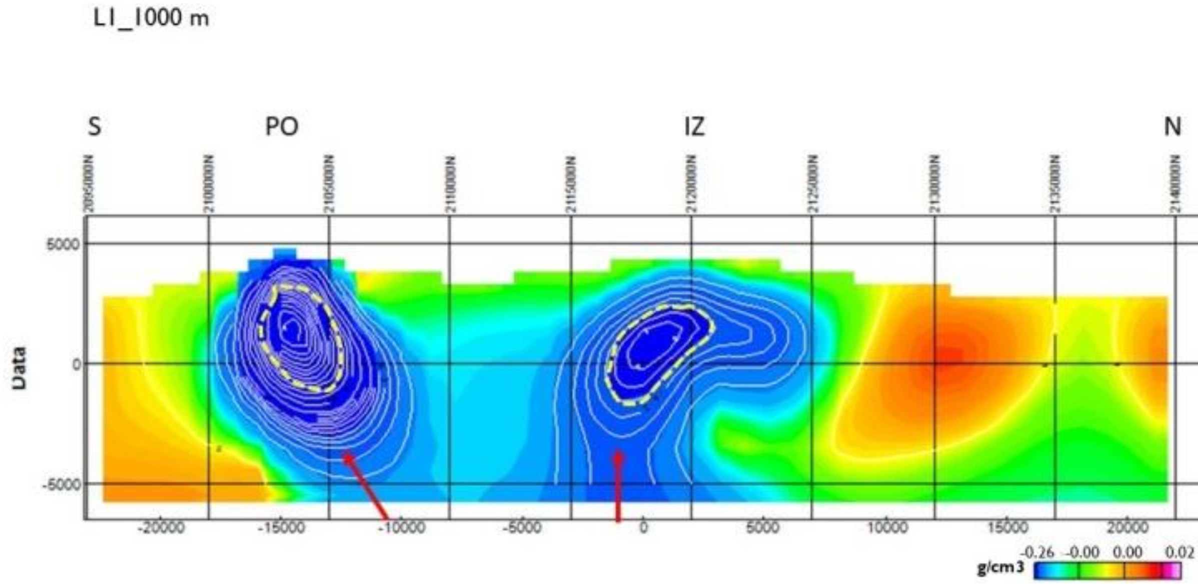

Figure 4 Cross-section in the N-S direction (L1) of the inverted density volume, resolution 1000 m, as shown in Figure 2, across Popocatépetl (PO) and Iztaccíhuatl (IZ) volcanoes. The dashed yellow lines surround the lowest density values, which we associate with the corresponding magma chambers; both are centered around 2000 m elevation and suggest they are fed by deeper magma sources, as indicated by the red arrows. The scale represents density contrast values relative to +2.67 g/cm^3. IZ is fed vertically whilst PO is fed at an angle, as shown by the arrows

The cross-section along L1 is presented in Figure 4; it was extracted from the density volume shown in Figure 3 and involves the two volcanic structures under consideration (PO, IZ) at a model resolution of 1000 m. The associated low-density regions show remarkable definitions of the chambers and the flow paths. The figure shows that both chambers are fed from a probably common, deeper magma source. PO hints at a single chimney reaching the surface, confirmed by the 3D inversions performed at various resolutions, whilst IZ presents an elongated shape extending ~8 km in the N-S direction, suggesting an explanation for the N-S stretched-out structure of this volcano, in which several summits extend along 6 km in the 126° azimuth. A vertical red arrow indicates the most likely feeding direction of the IZ magma chamber. There is a strong contrast between the elongated shape of the topographic structure of IZ and the conical shape of PO. The lower feeding conduits of the magmatic chamber of PO exhibit an angle of 21° from the vertical, as shown in Figure 4, rationalizing the southward migration of the volcanic activity. IZ is fed vertically; at sea level, the low-density region is deflected horizontally to the N, increasing its size in that direction, and constituting an oddity of that distribution, which will be further clarified when we discuss the higher-resolution cross-sections.

The cross-section along L2 appears in Figure 5; it was also extracted from the density volume shown in Figure 3; it crosses IZ from W to E. This projection shows a relatively narrow (~5 km), low-density conduit in IZ, connecting the bottom of the model to the summit; it appears to have cut through a high-density formation that flanks it along ~11 km on its eastern side and 4.5 km on its western side. What calls attention is not only the sharp boundary between low- and high-density regions but also their 5 to 10 km verticality. On the E side, there is another low-density anomaly (red arrow) whose maximum is located at -5 km elevation and in Figure 2 corresponds to the region of low-gravity value immediately E of IZ. The presence of this density minimum reinforces the idea that the region under extension in the E-W direction is being intruded by magmatic material; in fact, this density minimum seems to be another magma deposit that did not reach the surface.

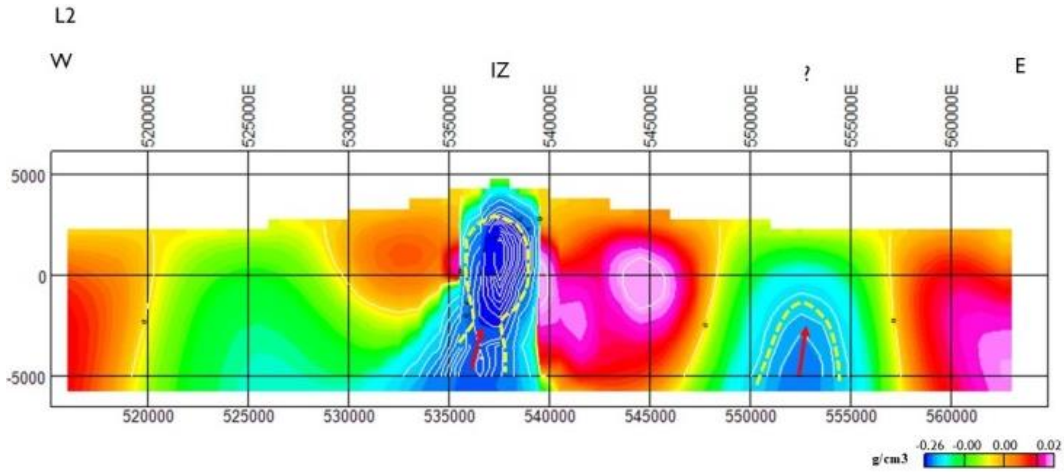

Figure 5 Cross-section in the E-W direction (L2) of the inverted density volume, 1000 m resolution, as shown in Figure 2, across the IZ volcano. The dashed yellow lines surround the lowest density values. In this projection, the central portion of the magma chamber appears directly connected to a deeper feeding source located below elevation -6 km, as indicated by the red arrow. There is a relevant, not outcropping low-density region to the E, whilst the western portion shows a wide, higher-density region flanked by high-density formations. The scale represents density contrast values relative to +2.67 g/cm^3

The cross-section along L3 is shown in Figure 6; it was extracted from the density volume shown in Figure 3; it crosses PO from W to E. In this projection the feeding trajectory of the low-density region appears vertical; the low-density region looks deflected to the E in its uppermost section, probably owing to the presence of a large portion of high-density material at the surface, immediately W of the summit. The sharp contrast between the low- and high-density regions is not as sharp as observed in IZ (Figure 5). The low-density region observed E of IZ is also present in the PO cross-section, although with higher density values; the low-density region to the W of IZ has disappeared in the W portion of the cross-section of PO.

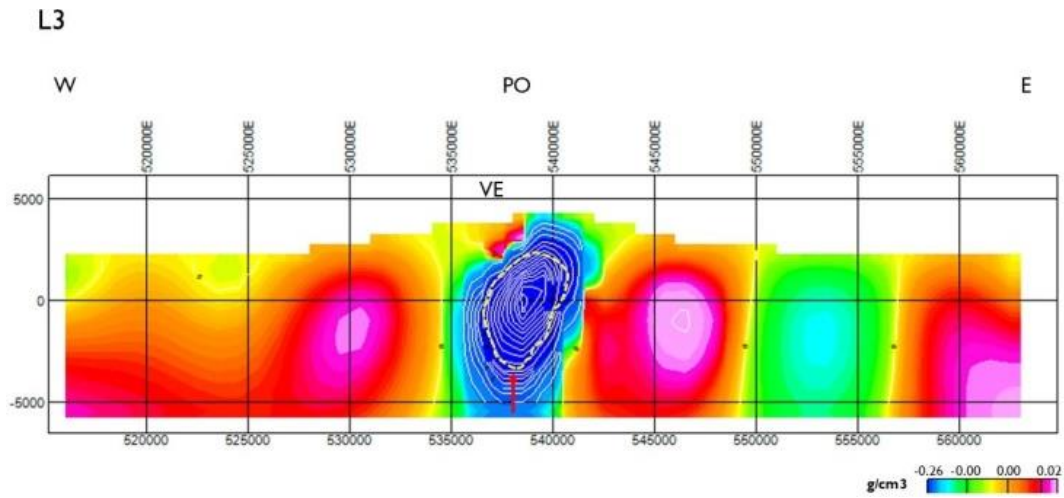

Figure 6 Cross-section in the E-W direction (L3) of the inverted density volume, 1000 m resolution, as shown in Figure 2, across the PO volcano. The dashed yellow lines surround the lowest density values that we associate with the melt zone; the red arrow indicates the feeding direction from a deeper chamber. In this projection, the lowest density value of the magma chamber appears centered at sea level (0 m elevation); to get the same depth for the minimum as in Figure 4 this cross-section should be obtained 3 km to the S. The high-density region on the N-side of PO, identified in Figure 3, appears also here, on the W-side of the cross-section of PO, and belongs to the extinct El Ventorrillo (VE) volcano. To the E, the relevant, low-density region shown in Figure 5 is also present, although here, the low-density region shallows. The scale represents density contrast values relative to +2.67 g/cm^3

The E-W cross-sections (Figures 5 and 6) show that PO and IZ low-density anomalies are well constrained by high-density material from -6 km to the surface; their widths are ~2.5 km. This observation contrasts with the anomaly widths registered in the N-S direction: 7-8 km for PO and 12 km for IZ along sea level, evoking deformed, disk-type distributions. This preliminary observation suggests that magma injection along the Sierra Nevada, including PO and IZ, has been occurring along a narrow, extended region in a nearly N-S direction since volcanic activity started in the Tláloc volcano at 1.8 Ma. VE corresponds to El Ventorrillo volcano, an ancestral version of Popocatépetl [29]; the high-density region corresponding to VE blocks what was the original chimney, deflecting activity towards the E, in this cross-section.

To illustrate the effects of resolution on a 3D inversion we performed a second inversion with a higher resolution (500 m) and extracted the corresponding cross-sections. In Figure 7 cross-sections were obtained from an inversion with 1000-m resolution and two with 500-m resolution; the length of the sections is directly proportional to the resolution; the former extends 50 km and the latter extends 25 km. Consequently, two 25-km cross-sections are needed to compare with the former.

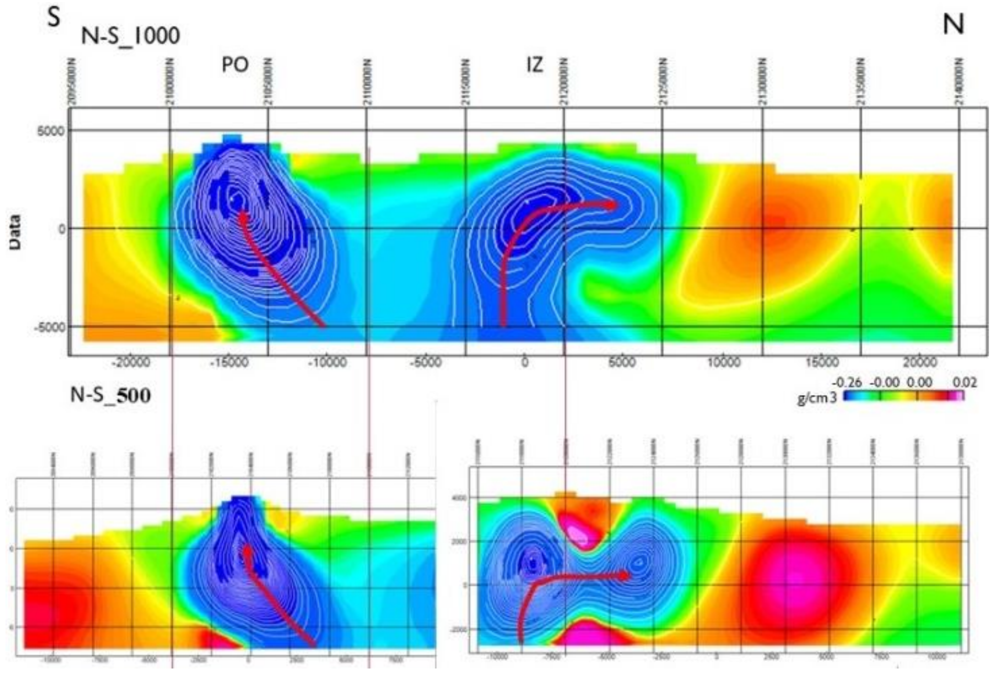

Figure 7 Comparison between sections obtained with resolutions of 1000 m (above) and 500 m (below) in the N-S direction. The horizontal scales are equal to allow for a direct comparison. Vertically, the former inversion extends down to an elevation of -6 km, while the latter reaches only -3 km. The geometries of the low-density regions change with the resolution since the size of the prisms used for each model changes; the models' topographic profiles improve with the higher resolution. The cross-sections are obtained over the same N-S line, as shown in Figure 2; the depth scale is the same for both lower figures. Arrows indicate the assumed flux directions. The higher resolution (500 m) presents more detail but a smaller penetration. We consider the 1000 and 500 m results are complementary. The scale represents density contrast values relative to +2.67 g/cm^3; the scale is valid for the three cross-sections

Although the same characteristics are maintained with both resolutions, the definition is better in the latter since the prisms used to approximate the actual structures are smaller. The resolution choice ultimately depends on the objective of the inversion; if a larger, deeper region needs to be surveyed lower resolutions are better. A combination of resolutions, as in the case presented, is recommended to better define shallow structures, and derive deeper relationships between surficial structures.

Cross-sections L1, L2, and L3 (1000-m resolution) were discussed above; we discuss now modifications introduced by the 500-m resolution in Figure 7. Depicted are two independent 3D inversions, one corresponding to PO and the second to IZ that have been placed under the L1 cross-section to simplify comparisons. Regarding PO, we appreciate that the chimney is better defined by the vertical contours; the observation that the chamber is fed at an angle is maintained, and its vertical shape appears elongated, defining more clearly the chimney's conduit. The minimum of the low-density anomaly is observed at +1500 m elevation. The changes experienced at IZ are more drastic; what appeared as an extended chamber appears now as two differentiated, interconnected chambers that we shall refer to as the North Chamber (NC) and the South Chamber (SC) of Iztaccíhuatl. In this projection, feeding of the NC appears to occur horizontally from the SC, in a passage that extends vertically from -1000 to +1000 m elevations. This configuration suggests that volcanic activity in the NC has been decreasing, and has, or soon could be terminated since horizontal feeding of the magma chamber intuitively appears more difficult than vertical feeding. An additional possible configuration is discussed further ahead. This horizontal, double-chamber volcanic configuration is peculiar. It explains the N-S elongation of the IZ volcanic edifice, referred to in the Nahuatl language as the White Woman, also referred to as the Sleeping Woman, identifying four peaks aligned in the SSE-NNW direction as the Head, the Chest, the Knees, and the Feet. The summit is in the Chest at 5230 m, with a vent that experienced eruptions in the Pleistocene and the Holocene. A possible crater, presently filled up with permafrost, has been reported in the second highest region of IZ (5050 m) identified as La Panza, corresponding to the area of Ayoloco glacier [6, 38]; given its location it may correspond to a vent of the volcano.

To determine whether we could establish the existence at depth of a deeper magma source, we performed an inversion decreasing the resolution from 1000 to 2500 m, reaching an elevation of -12 km as shown in Figures 8 and 9, or a depth of ~17 km from the summit of the volcanoes. The corresponding cross-sections were obtained along lines A and B (Figure 2). Figure 8 shows the low-density distribution along Line A, bifurcating to the S at -6 km elevation, from what seems to be the main magmatic feeder of IZ, to engender the PO magma chamber, centered at sea level; thus, the melt zone under IZ is likely the main feeding source for IZ and PO. The temperature vs pressure results [13] were obtained from the analysis of the clinopyroxenes of PO and are incorporated in Figure 8 into the density cross-section of Line A at the proper depths. Their deeper determinations must be located on the main magmatic source of both PO and IZ since there is no low-density region directly under PO at the corresponding depth.

North of IZ, a deeper bifurcation is present at -10 km elevation, which seems to occur at the upper portion of the deeper magma chamber; it corresponds to Telapón and Tláloc volcanoes. The melt zone below -10 km elevation is likely the main feeder for the whole Sierra Nevada volcanic activity. At the N end of the line, a low-density region rises to 2500 m above sea level (asl); we found no directly associated volcanic activity in the surface.

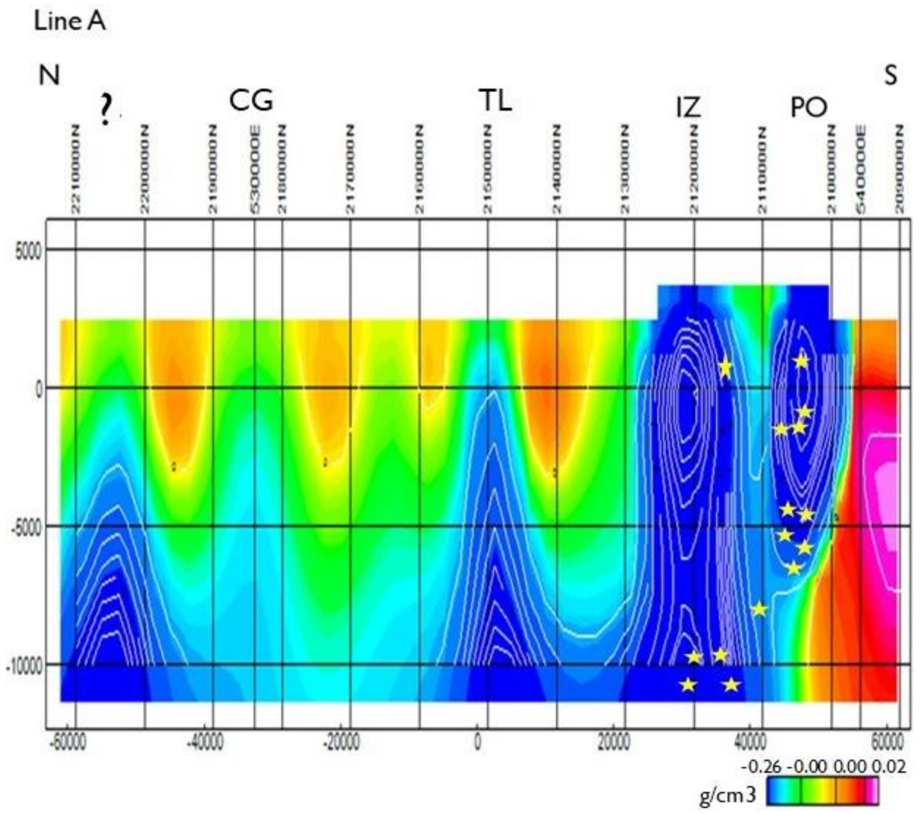

Figure 8 Cross-section along Line A (Figure 2) of 120 km length; depth reaches 12 km bsl. The low-density regions of PO and IZ reach the surface and are associated with their chimneys. The model resolution is 2500 m. A deeper bifurcation of the low-density anomaly is observed between IZ and TL. Stars denote geothermometer/geobarometer determinations [13]. PO, Popocatépetl. IZ, Iztaccíhuatl. TL, Tláloc. CG, Cerro Gordo. The scale represents density contrast values relative to +2.67 g/cm^3

Figure 9 shows the density distribution along Line B (Figure 2), with the same general characteristics as those in Line A. Line B crosses the Bouguer anomaly associated with IZ around 50 km N of its lowest value, ending past Malinche volcano; the latter structure will be analyzed elsewhere. Here, we will only note that along with its main volcanic chimney, there is a bifurcation to the NW of the low-density region, similar to that previously described for IZ and PO (Figure 9).

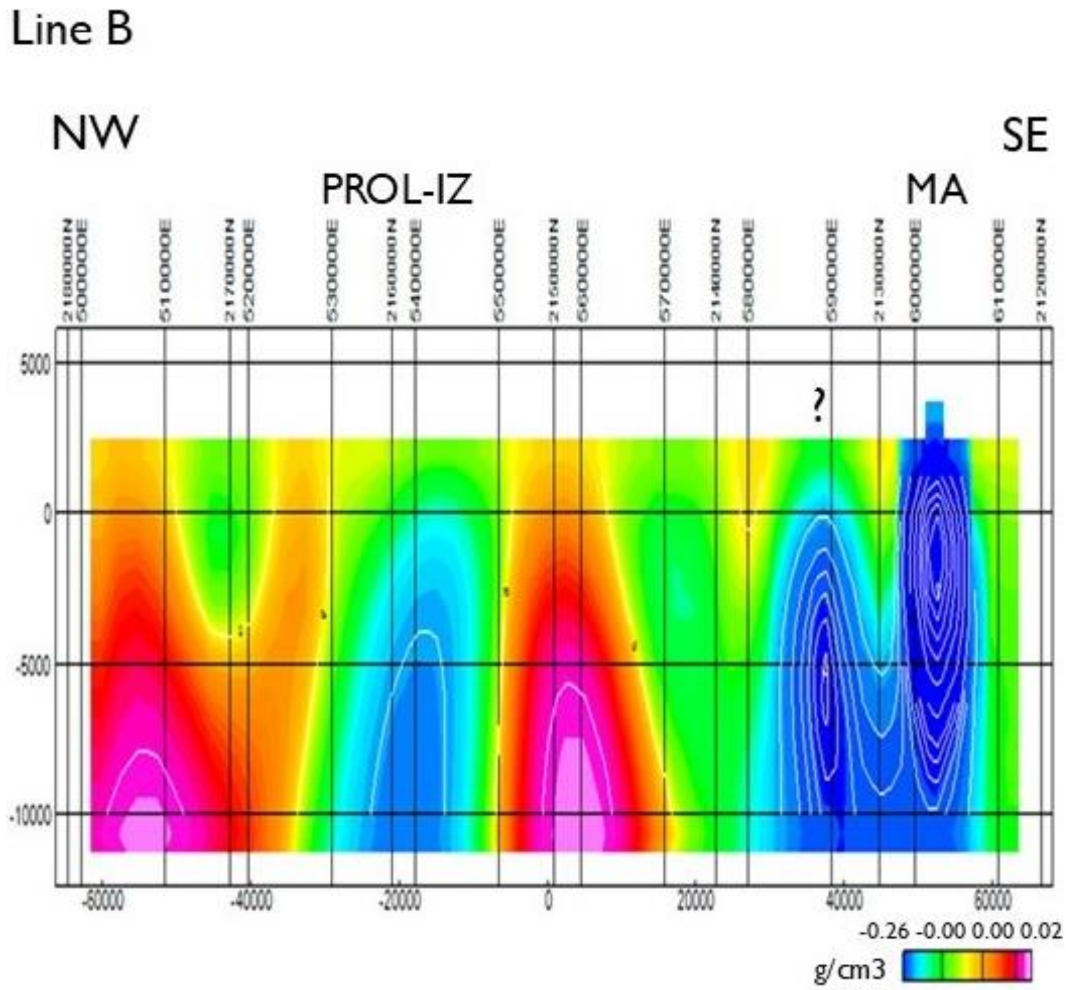

Figure 9 Cross-section along Line B (Figure 2); depth reaches 12 km bsl. This line intersects Malinche volcano (MA); adjacent to it is another low-density anomaly that does not reach the surface. Prol IZ, Prolongation of Iztaccíhuatl anomaly to the N. The scale represents density contrast values relative to +2.67 g/cm^3

4.3 Geosurfaces

Geosurfaces are density surfaces that delimit defined density ranges, helping visualize and measure the associated volumes. Three independent geosurfaces are shown in Figure 10, they delimit the regions where the density is <2.17 g/cm^3; that is, the regions in which magma reservoirs of PO and IZ have been located.

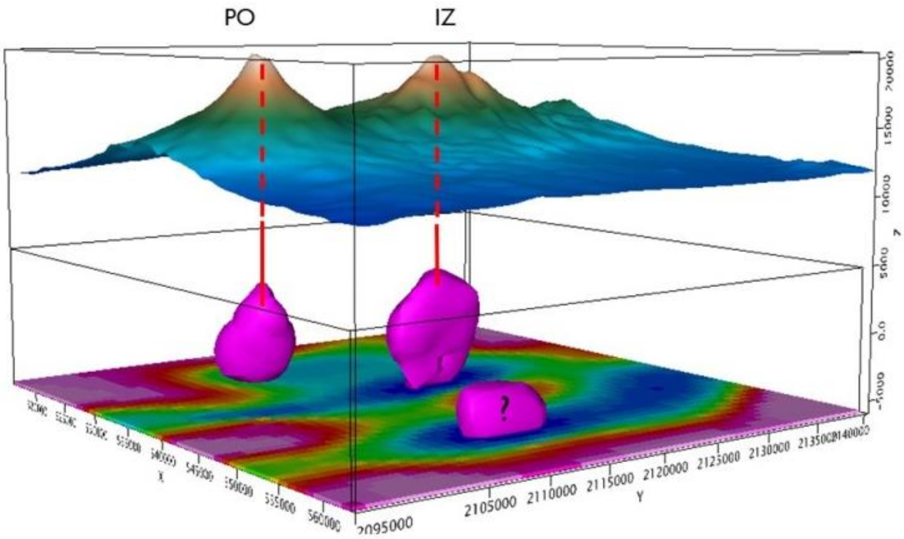

Figure 10 Isosurfaces containing densities <2.17 g/cm^3. Two of them correspond to the magma chambers of PO and IZ and the three reach the bottom of the model indicating continuation to greater depths; the one with the question mark terminates at elevation -2200 m. The DEM is displaced upwards to allow a clear vision of the isosurfaces. Red, dashed lines show vertical ties to the summits. The vertical scale of the lower box varies between -5000<Z<5000 m

4.4 Anomaly Depth Analysis

We now analyze six horizontal slices of the inverted density volume shown in Figure 3, appearing in Figure 11: elevation ranges from +1300 to -8000 m. The location of the three main volcanoes in the region PO, IZ, and MA at the +1300 m elevation shows three low-density regions associated with them. In Figure 7 the position of the magma chambers of PO and IZ was located at approximately this depth; we have not made an equivalent evaluation for MA but given the similarities with PO and IZ it would appear that analogous characteristics prevail. Alignment of high-density, N-S trending regions is observed throughout the western half of the map; on the eastern portion, these alignments are intercepted by similar NW-SE trending formations. Between PO-IZ and MA, such alignments exhibit a fair periodicity. This pattern persists to depths of -4000 m whilst the contrast increases between high- and low-density regions. Whether this implies that the extensional process reaches only to this depth requires of additional information, which is beyond the reach of the present study.

At the sea level section, the low-density region immediately E of the high-density region bounding the anomalies of PO and IZ increases its low-density value, corresponding to the already detected low-density region E of IZ and PO (Figures 5 and 6). It seems to confirm the suspicion that this is a magmatic intrusion that did not reach the surface. Starting at depths of -4000 m the high-density regions begin to coalesce, and the low-density regions connect in the N-S direction, confirming the observation made above regarding the existence of a single magma source for the whole Sierra Nevada.

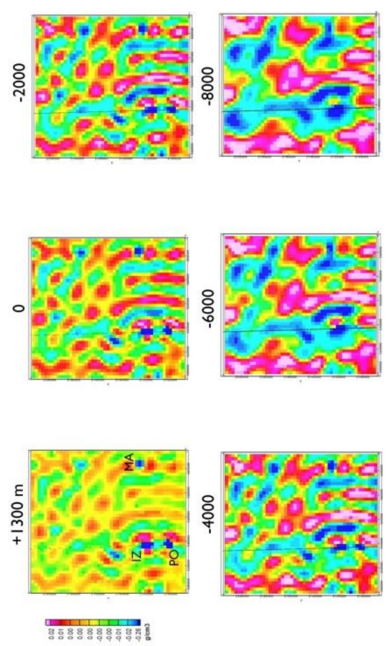

Figure 11 Horizontal planes at different depths show how density distributions vary with depth; in all sections, the north is in the upper part of the figure. The three major volcanic structures in the area are labeled PO, IZ, and MA; the latter corresponds to the Malinche volcano, located E of the former two volcanoes. An almost N-S-oriented line passing through the PO and IZ locations is visible in all these sections. The scale is valid for all sections; it represents density contrast values relative to +2.67 g/cm^3

4.5 The Extensional Process

We calculated the derivative Dx of the Bouguer anomaly (Figure 2) that is shown in Figure 12 to test for the periodicity in the E-W direction of the N-S alignments of the maxima and minima density positions, which evokes the idea of a horst and graben sequence in the region. The map in Figure 12 better defines what was already noted about the Bouguer anomaly; it confirms the alternation of high- and low-density gradients about the nearly N-S axis defined by the Sierra Nevada. We will call this, a gravity horst-and-graben arrangement, for its resemblance to the high and low topographic features of those geologic structures. This arrangement has not been previously described and appears to originate in a WNW-ESE extension process of the crust in this area; the change of concavity of these features at the Sierra Nevada lineament is remarkable, indicating that this is the tectonic axis of the extensional process.

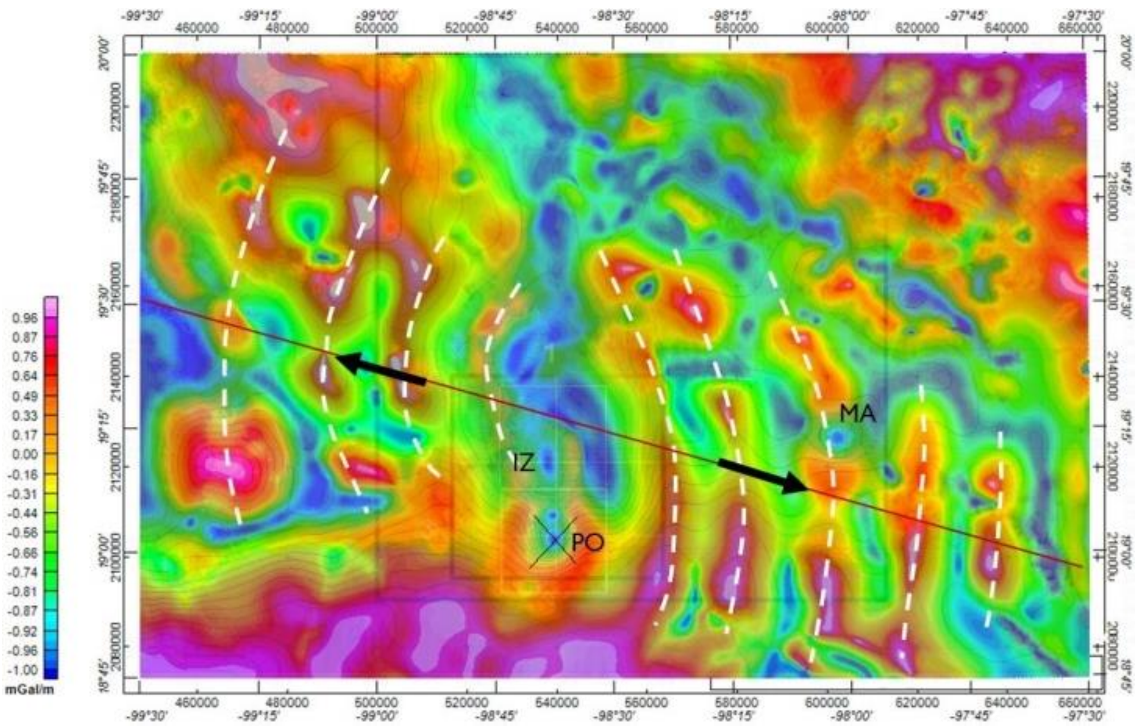

Figure 12 X-derivative of the Bouguer anomaly (Dx_BA) enhancing the pattern of alternating high- and low-values observed in the BA map of Figure 2; the X-axis is the horizontal one and the Y-axis is the vertical one. Dashed lines are superposed to the maxima; black arrows indicate the assumed tectonic extension direction. Faint lines and polygons are the same as in Figure 2; the WNW-ESE trending, red line across the map shows the axis of extension. IZ, Iztaccíhuatl volcano. PO, Popocatépetl volcano. MA, Malinche volcano

We note that the Malinche volcano disrupts the continuity of the high-density alignment it belongs to. The Malinche anomaly belongs to an additional group of NW-SE trending lows that parallel a similar group of low values to the north, which may indicate an additional extensional process in the SW-NE direction. Here, we just note their existence.

5 Density and Seismicity

There are few 3-D studies of the interior of PO and IZ to compare with the results presented here. A suitable one on PO [31], consists of a seismic tomography analysis in which the behavior of the Vp/Vs ratio is described. To perform the comparison, we obtained the corresponding density cross-sections from the inverted density volume in Figure 3; their location is displayed in Figure 12 as two lines in X over PO. Figure 13 compares the SW-NE density cross-section with the A1-B1, Vp/Vs results; the horizontal and vertical scales are equal for both data sets, extending down to -3 km elevation, the depth reached by the density model of 250-m resolution. This is the highest resolution attained in this study. Based on variations in density gradients within the low-density region, we trace a channel (dashed lines) extending from the summit to the bottom of the density model; this channel exhibits a minimum at +1 km elevation that we interpret as the upper magma chamber of PO. This location receives magmatic material from a deeper source and ejects it through the channel's upper portion, identified with the volcanic chimney of PO.

From the report based on local earthquake seismic tomography [31], we extracted a simplified version of their A1-B1, Vp/Vs ratio, as shown in Figure 13, where the same dashed lines in the density cross-section are placed over the seismic results, showing that the conduit fits intermediate (i.e., 1.80≤Vp/Vs≤1.90) values (white regions), exhibiting a fair correlation with the density-defined channel.

Density and Vp/Vs results are presented in the NW-SE cross-sections of Figure 14. Again, horizontal and depth scales are the same in both illustrations. The density cross-section shows that contours in the low-density region exhibit variations that allow for the definition of a central channel, enhanced by two dashed lines; in this projection, the channel varies in width between 1 and 2 km, extending from the bottom of the model (-3 km) to the summit of PO. We identify the chimney of PO as the portion of this channel above +2 km; below -1 km, we interpret it as the conduit that feeds the magma chamber from a deeper reservoir, and between -1 and +2 km we locate the magma chamber.

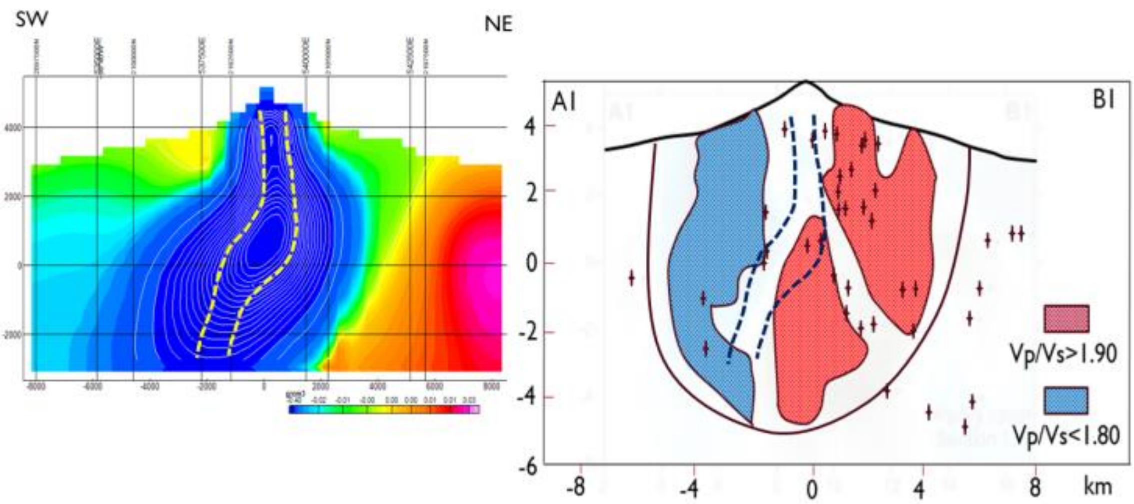

Figure 13 Comparison of the SW-NE density cross-section (250-m resolution) across PO with the seismic Vp/Vs ratios [31]. The location of the cross-section is shown in Figure 12, as an X over PO, which corresponds to the A1-B1 seismic cross-section. Vertical and horizontal axes are equal in both data sets. The dashed lines in the density section show the inferred conduit that transports magmatic material to the chamber, just above sea level, and from there to the surface, through the chimney; a deflection is registered to the NE. The same dashed lines are superposed in the seismic results, showing that the conduit fits intermediate (i.e., 1.80≤Vp/Vs≤1.90) values (white regions). Crosses represent hypocenters and areas outside the seismic network, where the resolution was lower, are masked. Stars indicate the location of tremors. The density scale represents contrast values relative to +2.67 g/cm^3 and varies slightly from the previous scales owing to the higher model resolution

The low-density region (blue) is constrained by two, adjacent high-density regions. The high-density region (VE) on the NW slope of PO's edifice blocks the low-density region deviating the trajectory of the central channel. We identify this region with a relict version of PO, El Ventorrillo, that was abandoned [29], deflecting the chimney to the SE, as shown in Figure 14, creating a high-density, high-Vp/Vs region in its place. The oldest lava from VE are dated at 330 ka from $^{40}Ar/^{39}Ar$ determinations [29]. It was proposed [30] that El Ventorrillo was destroyed at 14.1 ka by a catastrophic event and the present cone of PO began its construction. Our interpretation of the results in Figure 14 complements their analysis.

The dashed lines showing the chimney ́s trajectory are copied to the A2-B2 seismic cross-section, where they display a remarkable coincidence with the vertical channel defined between the Vp/Vs>1.90 regions. The fact that the seismic and the density models coincide in such identification reinforces the results of both methodologies.

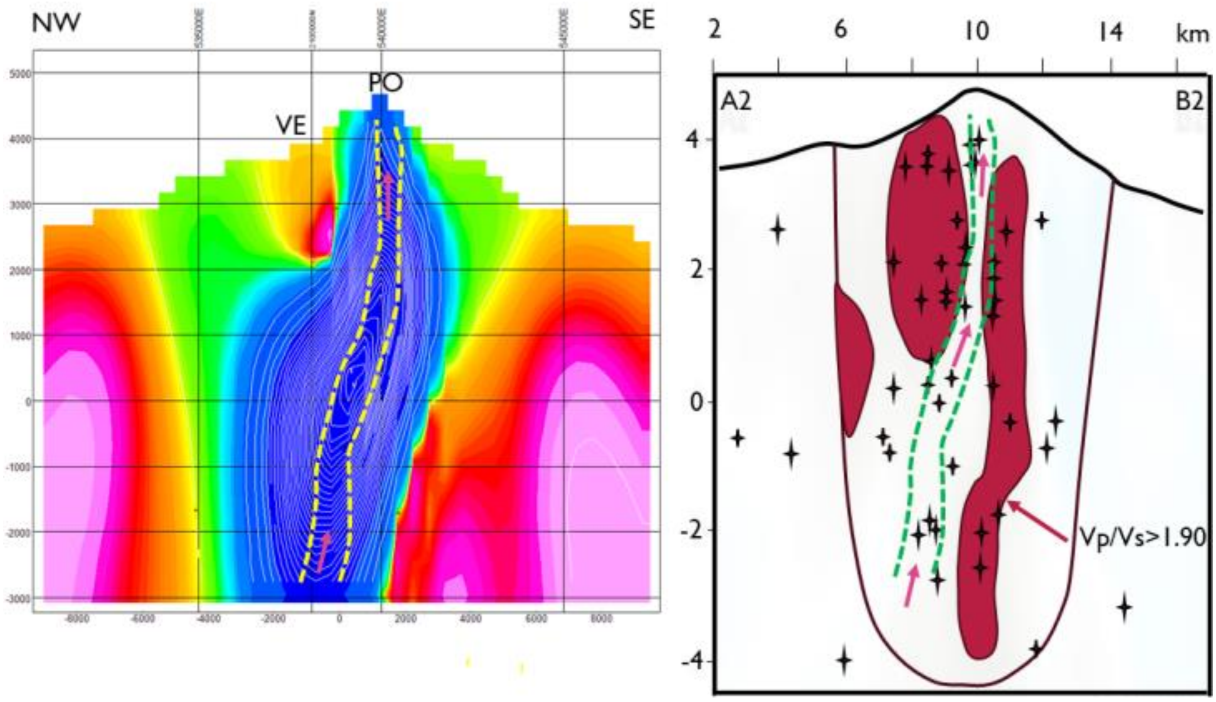

Figure 14 Comparison of the NW-SE density cross-section (250-m resolution) across PO with the Vp/Vs ratio [31] along the same cross-section (A2-B2). The vertical and horizontal axes are equal. The trace of the cross-section is shown in Figure 12, as an X over PO; the NW-SE line corresponds to this illustration. Two dashed lines highlight a low-density channel (left) that is then superposed to the Vp/Vs diagram, showing an outstanding correlation, particularly above sea level, with the region of low Vp/Vs values defining the low-density channel. El Ventorrillo (VE) is an ancestral version of the present PO volcano, that became a high-density, high-Vp/Vs region. Stars represent the hypo-central location of the earthquakes reported in the seismic study. The density scale is the same as that in Figure 13

6 PO Chimney's 3D View

A 3D view of the low-density region (Figure 15) was obtained following the same procedure as that in Figure 10 allowing us to infer that the chimney, at an elevation of +3000 m, in the N-S direction may be as narrow as 100 m, and in some places, it may be less; it extends in the E-W direction for 300 to 400 m, and from 400 to 500 m in the vertical direction. We shall call it the Popocatépetl Occlusion since it represents the blocking of the central passage of magmatic materials to the surface. The importance of this finding is that this narrow conduit may eventually be blocked, preventing the exhaust of the rather continuous activity of this volcano. This in turn may force a new exhaust trajectory that may include explosive activity in the flanks of the present structure, potentially threatening the neighboring, densely populated areas. We speculate that the conduit feeding the ancestral, El Ventorrillo volcano, already contained a similar occlusion region, which was blocked, deflecting the activity to create the present cone of PO.

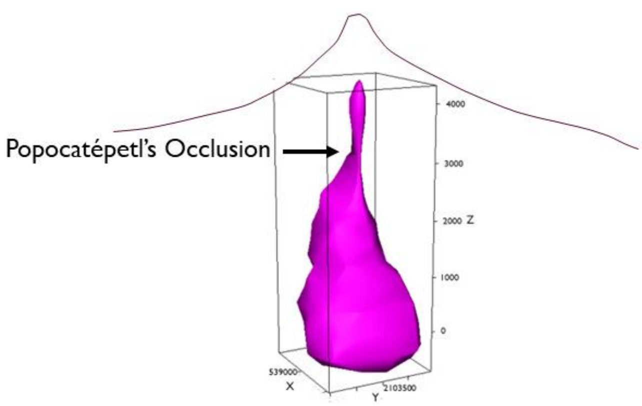

Figure 15 Envelope of the low-density (≤ 2.05 g/cm^3) surface above sea level obtained from the inverted volume of PO at 250-m resolution. At +3000 m the chimney thins out in the N-S direction to 100 m or less and is extended 300 to 400 m in the E-W direction. At +4000 m its X-Y dimensions experience a slight increment before reaching the summit

7 Discussion

Performing a 3D inversion on the area of PO and IZ we found that PO's upper magma deposit is fed at an angle, not vertically; when the resolution was decreased and penetration incremented, we realized that PO and IZ have the same, deeper chamber feeding both volcanoes. We inferred that around -10 km appeared the top of the deeper magmatic layer. Upon increasing the resolution, we discovered that the elongated magma chamber of IZ became a double magma chamber, with the unexpected result that the main chamber is fed vertically, while the adjacent chamber to the N is apparently fed horizontally from the main chamber.

Although horizontal feeding cannot be discarded, we believe that another sequence of events is more likely to have occurred: Given the southward migration of activity in the Sierra Nevada, the north chamber of IZ appeared first and was fed vertically at that time, giving rise to the north portion of the present structure of IZ. Subsequently, activity migrated to the south, abandoning this magma chamber and forming the southern one, which was, and continues to be, fed vertically, creating the elongation to the south of this volcano. The chambers now appear to be connected horizontally at their widest points, finally giving the appearance that the southern chamber feeds horizontally the northern one. With the present data we cannot discern which of the interpretations should prevail.

Since the early descriptions of the distribution of the Sierra Nevada range, it was proposed that the volcanic alignment was induced by “a secondary crack” [32, 33]. Here, we identify an extensional process whose axis corresponds with the Sierra Nevada and extends to the ESE and WNW in the form of alternating gravity maxima and minima, as shown in Figure 12. It appears that this extensional process is responsible for the southward migration of the volcanic activity in the Sierra Nevada. Furthermore, to the W, this tectonic process affects the Mexico City area. At the same time, to the E it upsets the City of Puebla, to name the most important human conglomerates in the area. We believe that the suggestion concerning the secondary role that regional crustal tectonics has played in the N-S alignment of the volcanoes [5] should be revised, considering the extensional phenomenon reported in this study.

We identify a deviation of the exhaust chimney of PO (Figures 13-15) caused by a high-density formation near and up to the surface of the cone of PO. We link this high-density formation with an ancestral version of PO called El Ventorrillo. The new discharge trajectory gave rise to the present volcanic edifice of PO. Then we assembled a 3D version of the present exhaust chimney, finding that it has a very narrow section at the +3000 m elevation, which we named the Popocatépetl’s Occlusion, indicating that it runs the risk of becoming clogged, which would give rise to a new exhaust trajectory. It appears that a similar occlusion of the chimney already occurred in El Ventorrillo at 14.1 ka.

A comparison was performed between seismic results (Vp/Vs) [31] and the density distribution with a resolution of 250 m (Figures 13 and 14); The low-density channel transporting magmatic materials, first to PO’s magma chamber and then up to the summit through the chimney, is then superposed on the seismic results where good matches are observed with the Vp/Vs cross-sections. It appears that after abandonment, El Ventorrillo became a high-density, high-Vp/Vs section.

The 3D inversion at 2500-m resolution along Lines A and B (Figures 8 and 9) reached -12 km elevation, revealing the upper portion of the deeper magma chamber feeding IZ and PO. It requires that the geothermometric/geobarometric determinations [13] at depths ≤8 km bsl be located in the upper portion of such a chamber since the Popocatépetl low-density distribution does not reach such depths.

8 Conclusions

This study revealed that PO and IZ are fed by a magma chamber that starts at -10 km bsl, or deeper, showing that IZ is nourished vertically from this chamber, whilst PO is fed at an angle of 21° from the vertical. A bifurcation to the S, of the low-density region associated with IZ occurs at -6 km bsl, which gives rise to the PO shallow magma deposit. At a resolution of 1000 m, the IZ model shows a deflection to the N of the low-density region; however, when the resolution is lowered to 500 m, the low-density distribution reveals the existence of two chambers: the South Chamber is fed vertically from a deeper source, while the North Chamber appears to be fed horizontally from the former. Whether the North Chamber was originally fed vertically and at some stage, activity migrated to the S, closing the vertical feed, and displacing it to its present location requires further studies of this phenomenon. In our experience, the lateral magma feed discussed here is a most unusual effect that will probably be discarded in favor of the alternate sequence of events sketched above.

The lower-resolution, deeper-penetration inversion indicates the presence of a lower magma chamber that seems to have fed the whole Sierra Nevada eruptive process. The top of the chamber is located at -10 km bsl. The geothermometric results [13] show consistency with the low-density distribution obtained from the inversion process. A comparison is also made with the shallower seismic results [31] and the corresponding low-density cross-sections where the same discharge trajectory is identified in both studies.

An extensional process is identified in the WNW-ESE direction, where the extensional axis lies along the Sierra Nevada range and expands beyond the Mexico City area to the NW and Malinche volcano to the SE. Despite its great tectonic relevance, the origin and significance of this extensional process cannot be dealt with in this presentation.

Finally, we identified a region of the chimney of PO that is reduced in dimensions, making it likely to be shut, creating a potentially explosive scenario. We argued that this process may have already happened in the case of El Ventorrillo volcano, an ancestral version of PO, that at 14.1 ka gave rise to the present edifice of Popocatépetl.

Acknowledgments

During the development of this work, MC received support from Consejo Nacional de Ciencia y Tecnología (CONACYT), Mexico. We thank Posgrado en Ciencias de la Tierra, UNAM, for access to computational resources. This study has been supported by IIMAS, UNAM; we acknowledge material support from the three institutions. We acknowledge the meticulous review of the manuscript by the anonymous reviewers.

Conflicts of Interest

The authors declare that the research was conducted in the absence of any commercial or financial relationships.

References

[1] Suny é-Puchol, I. Hodgetts, AGE, Watt, SFL, Arce, JL, Barfod, DN, Mark, DF, Giovanni Sosa-Ceballos, G, Siebe, C, Dymock, RC, Blaauwh, M. (2022) Reconstructing the middle to late Pleistocene explosive eruption histories of Popocatépetl, Iztaccíhuatl and Tláloc-Telapón volcanoes in Central México, J. Volc. Geothermal Res. Volume 421, January 2022, 107413, https://doi.org/10.1016/j.jvolgeores.2021.107413

[2] Martín Del Pozzo, A. L., Rodríguez, A., Portocarrero, J., (2016) Reconstructing 800 years of historical eruptive activity at Popocatépetl Volcano, Mexico. *Bull. Volcanol.* 78, 1.

[3] Mangler, M. F., Petrone, C. M., Hill, S., Delgado-Granados, H., Prytulak, J., 2020. A pyroxenic view on magma hybridization and crystallization at Popocatépetl volcano, Mexico. Front. Earth Sci. 8, 1–22. https://doi.org/10.3389/feart.2020.00362

[4] Macías J. L. Arce, J. L., García-Tenorio, F., Sosa-Ceballos, G., Gardner, J. E., (2020) Source and behavior of pyroclastic density currents generated by Vulcanian-style explosions of Popocatépetl volcano (Mexico) on 22 January 2001. https://doi.org/10.1016/j.jvolgeores.2020.107071

[5] Cadoux, A., Missenard, Y., Martinez-Serrano, R. G., Guillou, H., (2011). Trenchward Plio-Quaternary volcanism migration in the Trans-Mexican Volcanic Belt: the case of the Sierra Nevada range. *Geol. Mag*. 148, 492–506. https://doi.org/10.1017/S0016756810000993

[6] Delgado-Granados, H. P. Julio Miranda, R. Alvarez, E. Cabral-Cano, L. Cárdenas-González, F. Correa-Mora, M. Luna Alonso, and C. Huggel (2005). Study of Ayoloco glacier at Iztaccíhuatl volcano (Mexico): hazards related to volcanic activity-ice cover interactions. Z. Geomorph. N. F., Suppl. Vol. 140, 181-193. Jul. 2005.

[7] Muñoz-Salinas, E., Castillo-Rodríguez, M., Manea, V., Manea, M., Palacios, D., (2009). Lahar flow simulations using LAHARZ program: application for the Popocatépetl volcano, Mexico. *J. Volcanol. Geotherm. Res.* 182 (1–2), 13–22.

[8] Macías, J. L., Arce, J. L., García-Tenorio, F., Layer, P. W., Rueda, H., Reyes-Agustín, G., López-Pizaña, F., Avellán, D,, (2012) Geology and geochronology of Tláloc, Telapón, Iztaccíhuatl, and Popocatépetl volcanoes, Sierra Nevada, Central Mexico. Geol. Soc. Am. Field Guide 25, 163–193. https://doi.org/10.1130/2012.0025(08)

[9] Macías-Vázquez, J. L., Carrasco-Núñez, G., Delgado-Granados, H., Martin-del Pozzo, A. L., Siebe-Grabach, C., Hoblitt, R. P., Sheridan M. F., Tilling, R. I., Bonifaz, R., Cabrera, A. L., Alvarez, R., (1995), Mapa de peligros del volcán Popocatépetl, escala 1:250,000: México, D. F. Universidad Nacional Autónoma de México. Instituto de Geofísica. 1 mapa.

[10] De la Cruz-Reyna, S., Siebe, C. (1997). The giant Popocatépetl stirs. *Nature*, 388, 227.

[11] García-Tenorio, F., 2002, Stratigraphy and petrography of Iztaccihuatl volcanic complex, (In Spanish). Instituto Politécnico Nacional, Escuela Superior de Ingeniería y Arquitectura, Unidad Ticomán, Tesis profesional, 149 p.

[12] Alvarez, R., & Camacho, M. (2024). The N-S Extension of The Mexico Basin is Confirmed by Gravity Analysis. *Transactions on Engineering and Computing Sciences*, 12(3). https://doi.org/10.14738/tecs.123.17139

[13] Tommasini, S., Bindi, L., Savia, L. Mangler, MF, Orlando, A., Petrone, CM. (2022) Critical assessment of pressure estimates in volcanic plumbing systems: The case study of Popocatépetl volcano, Mexico. *LITHOS* 408-409 (2022) 106540. https://doi.org/10.1016/j.lithos.2021.106540

[14] Mangler, M. F., Prytulak, J., Gisbert, G., Delgado-Granados, H., Petrone, C. M., (2019). Interplinian effusive activity at Popocatépetl volcano, Mexico: new insights into evolution and dynamics of the plumbing system. Volcanica 2, 45–72. https://doi.org/10.30909/vol.02.01.4572

[15] Hirt, C, S. J. Claessens, T. Fecher, M. Kuhn, R. Pail, M. Rexer (2013), New ultra-high resolution picture of Earth's gravity field, Geophysical Research Letters, Vol 40, https://doi.org/10.1002/grl.50838

[16] Camacho M, Alvarez R (2021) Geophysical modeling with satellite gravity data: EIGEN6C4 vs GGMplus. *Engineering*, 13, 690-706. https://doi.org/10.4236/eng.2021.1312050

[17] Alvarez, R. & Yutsis, V. (2015) Southward migration of magmatic activity in the Colima Volcanic Complex, Mexico: An ongoing process. *International Journal of Geosciences*, 6, 1077-1099. http://dx.doi.org/10.4236/ijg.2015.69085

[18] Guevara-Betancourt, R., Yutsis, V., Varley, N., Almaguer, J., Alvarez, R., Calderón-Moctezuma, A., and Sieck, P. (2023) Insights into the plumbing system of Colima Volcanic Complex. *J. Volcanol. Geothermal Res*., 2022 433 (2023) 107711. https://doi.org/10.1016/j.jvolgeores.2022.107711

[19] Alvarez, R. & Camacho, M. (2023a) The plumbing system of the Hunga Tonga Hunga Ha'apai volcano, *Journal of Earth Science*, Vol. 34, No. 3, p. 706-716, June 2023. https://doi.org/10.1007/s12583-022-1792-0

[20] Alvarez, R. & Camacho, M. (2023b). Applying high-resolution gravity analysis to volcanic plumbing systems: the case of Nevado de Toluca volcano, Mexico. *Transactions on Engineering and Computing Sciences*, 11(4). 184-207. https://doi.org/10.14738/tecs.114.15392

[21] Hirt, C., W. E. Featherstone and U. Marti (2010), Combining EGM2008 and SRTM/DTM2006.0 residual terrain model data to improve quasigeoid computations in mountainous areas devoid of gravity data, J. Geod., 84(9): 327 557-567, https://doi.org/10.1007/s00190-010-0395-1

[22] Linares, F. & Arraiz, D. & Orihuela, N. (2016). Mapa de anomalías de Bouguer de Venezuela derivado del modelo combinado EIGEN-6C4. Geociencias Aplicadas Latinoamericanas. https://doi.org/10.3997/2352-8281.20150006

[23] Forsberg, R. (1984), A study of terrain reductions, density anomalies and geophysical inversion methods in gravity field modelling, Report 355, Department of Geodetic Science and Surveying, Ohio State 783 University, Columbus.

[24] Hirt, C. (2010), Prediction of vertical deflections from high-degree spherical harmonic synthesis and residual terrain model data, J. Geod., 84 (3), 179-190. https://doi.org/10.1007/s00190-009-0354-x

[25] Ryan, W. B. F., Carbotte, S. M., Coplan, J. O., O'Hara, S., Melkonian, A., Arko, R., Weissel, R. A., Ferrini, V., Goodwillie, A., Nitsche, F., Bonczkowski, J., Zemsky, R., (2009). Global multi-resolution topography synthesis. *Geochem. Geophys. Geosyst.* 10, Q03014 https://doi.org/10.1029/2008GC002332

[26] Macleod, I. N. & Ellis, R. G., 2013. Magnetic vector inversion, a simple approach to the challenge of varying direction of rock magnetization. Australian Society of Exploration Geophysicists, Extended Abstracts 2013, 1–4. Melbourne.

[27] Ellis, R. G., de Wet, B., and Macleod, I. N., 2012. Inversion of magnetic data from remanent and induced sources. ASEG Extended Abstracts 2012 (1), 1–4. https://doi.org/72672772810.1071/ASEG2012ab117

[28] Ingram, D. M., Causon, D. M., Mingham, C. G., 2003. Developments in Cartesian cut cell methods. Math. Comput. Simulat. 61 (3–6), 561–572. https://doi.org/10.1016/S03784754(02)00107-6

[29] Sosa-Ceballos, G., Macías, J. L. García-Tenorio, F., Layer, P., Schaaf, P, Solís-Pichardo, G., Arce J. L. (2015). El Ventorrillo, a paleostructure of Popocatépetl volcano: insights from geochronology and geochemistry. *Bull Volcanol.* 77: 91. https://doi.org/10.1007/s00445-015-0975-2

[30] Sosa-Ceballos G, Gardner JE, Siebe C, Macias JL (2012) A caldera-forming eruption ~14100 14C yr BP at Popocatépetl volcano, México. Insights from eruption dynamics and magma mixing. *J. Volcanol Geotherm Res* 213–214: 27–40.

[31] Kuznetsov, P. Y., Koulakov, I. Y., (2014). The three-dimensional structure beneath the Popocatépetl volcano (Mexico) based on local earthquake seismic tomography. *J. Volcanol. Geotherm. Res.* 276, 10–21. https://doi.org/10.1016/j. jvolgeores.2014.02.017

[32] Felix, J. & Lenk, H. (1890) Beitraege zur Geologie und Paleontologie: Leipzig: A. Felix: Stuttgart: E. Schweiterbartsche Verlagshandlung, 142 p.

[33] Macías, JL (2005) Geología e historia eruptiva de algunos de los grandes volcanes activos de México. Boletín de la Sociedad Geológica Mexicana, Volumen Conmemorativo del Centenario, Temas Selectos de la Geología Mexicana, Tomo LVII, Núm. 3, 2005, p. 379-424.

[34] Hirt, C. (2013), RTM gravity forward-modeling using topography/bathymetry data to improve high degree global geopotential models in the coastal zone, Marine Geod., 36(2): 1-20, 789. https://doi.org/10.1080/01490419.2013.779334

[35] Siebe, C., Macías, J. L., (2006). Volcanic hazards in the Mexico City metropolitan area from eruptions at Popocatépetl, Nevado de Toluca, and Jocotitlán stratovolcanoes and monogenetic scoria cones in the Sierra de Chichinautzin Volcanic Field. Spec. Pap. Geol. Soc. Am. 402, 253.

[36] Martin-Del Pozzo, A. L., Cifuentes, G., Cabral-Cano, E., Bonifaz, R., Correa, F., Mendiola, I. F., (2003). Timing magma ascent at Popocatépetl volcano, Mexico, 2000–2001. *J. Volcanol. Geotherm. Res*. 125 (1–2), 107–120.

[37] Nixon, G. T., (1989) The Geology of Iztaccíhuatl Volcano and Adjacent Areas of the Sierra Nevada and Valley of Mexico. Geological Society of America, Special Paper no. 219 (58 pp).

[38] Alvarez, R. and H. Delgado (2002) Characterization of a tropical ice body on Iztaccíhuatl volcano, Mexico. In Proceedings of SPIE Vol. 4758. Ninth International Conference on Ground Penetrating Radar, S. K. Koppenjan and H. Lee, Editors, pp 438-442, 2002.